Charge states and energy loss of 300-MeV/u U^{73+} ions channeled in a silicon crystal

D. Dauvergne,[1] C. Scheidenberger,[2] A. L'Hoir,[3] J. U. Andersen,[4] S. Andriamonje,[5] C. Böckstiegel,[6] M. Chevallier,[1] C. Cohen,[3] N. Cue,[7] S. Czajkowski,[2] J. S. Forster,[8] H. Geissel,[2] H. Irnich,[2] T. Kandler,[2] R. Kirsch,[1] A. Magel,[9] P. H. Mokler,[2] G. Münzenberg,[2] F. Nickel,[2] Yu. L. Pivovarov,[10] J-C. Poizat,[1] M. F. Politis,[3] J. Remillieux,[1] D. Schmaus,[3] Th. Stöhlker,[2] T. Suzuki,[2] and M. Toulemonde[11]

[1] *Institut de Physique Nucléaire de Lyon and IN2P3, Université Claude Bernard Lyon-I, 43, Boulevard du 11 Novembre 1918, 69622 Villeurbanne Cedex, France*

[2] *Gesellschaft für Schwerionenforschung mbH Darmstadt, Planckstrasse 1, D-64291 Darmstadt, Germany*

[3] *Groupe de Physique des Solides, CNRS UMR 7588, Université Paris 7 et Paris 6, 75251 Paris Cedex 05, France*

[4] *Institute of Physics and Astronomy, University of Aarhus, DK 8000 Aarhus C, Denmark*

[5] *Centre d'Etudes Nucléaires de Bordeaux-Gradignan and IN2P3, le Haut-Vigneau, 33175 Gradignan Cedex, France*

[6] *Institut für Kernphysik, Technische Hochschule Darmstadt, Schlossgartenstrasse 9, D-64289 Darmstadt, Germany*

[7] *Department of Physics, The Hong Kong University of Science and Technology, Kowloon, Hong Kong*

[8] *Engineering Physics Department, McMaster University, Hamilton, Ontario, Canada L8S 4M1*

[9] *Universität Giessen, Heinrich-Buff-Ring 16, D-35392 Giessen, Germany*

[10] *Nuclear Physic Institut, P.O. Box 25, 634050 Tomsk, Russia*

[11] *Centre Interdisciplinaire de Recherche avec les Ions Lourds, UMR 11 CNRS-CEA, rue Claude Bloch, 14040 Caen Cedex, France*

(Received 11 June 1998; revised manuscript received 21 October 1998)

We have studied the emerging charge states q_{out} and energy loss of 300-MeV/u U^{73+} incident ions transmitted along a $\langle 110 \rangle$ axis of a 120-μm-thick Si crystal. The emerging charge state distribution $F_C(q_{out})$ for well-channeled ions is governed mainly by electron impact ionization (EII). The corresponding EII cross sections were obtained by fitting the experimental $F_C(q_{out})$ with Monte Carlo simulations. For M shell ionization, they were found to be twice larger than those given by the binary encounter dipole approximation. The measured energy loss spectra were also compared to Monte Carlo simulations. The mean values and widths of these spectra increase with q_{out}, reflecting the increase of the stopping power S with increasing transverse energy $E_\perp$. The measured stopping for channeled ions with frozen charge state 73+ and for nonchanneled ions with charge state close to 90+ is in good agreement with theoretical estimates. Owing to the very high ion velocity, there is a significant contribution (25%) to the stopping from Si-L shell excitation even for the best channeled ions. The width and the asymmetrical shape (skewness μ) of the energy-loss spectra depend strongly on q_{out}($\mu>0$ for very well-channeled ions, $\mu<0$ for poorly channeled ions). For well-channeled ions, energy-loss spectra were reproduced by Monte Carlo simulations with the $S(E_\perp)$ curve extracted from fitting the mean energy losses. [S1050-2947(99)01604-2]

PACS number(s): 61.85.+p, 34.80.Dp

I. INTRODUCTION

Channeling of swift ions allows detailed investigations of energy loss and other atomic-collision processes such as ionization, excitation, and capture for such ions, under restricted impact parameters. In particular, by a selection of particles with low transverse energy $E_\perp$, one may suppress all atomic processes involving the target nuclei, such as mechanical electron capture (MEC) and nuclear impact ionization (NII), and to some extent one may isolate the contribution of valence electrons from that of core electrons for processes such as ionization, excitation, capture, and energy loss. Particles with well-defined $E_\perp$ may be selected in various ways. One can take advantage of the fact that, for ions of given velocity v and charge state q, the energy-loss spectrum $g(\Delta E)$ of the channeled beam is broad, reflecting the dependence of the stopping power $S(E_\perp)$ on transverse energy $E_\perp$ [1]. The $E_\perp$ selection is here performed through a selection in energy loss. This procedure may be used in experiments with incoming bare or nearly bare ions at high energy: in this case, the dominant charge exchange process is target electron capture [radiative electron capture (REC) [2], dielectronic recombination [3]), but the corresponding cross sections are small enough to ensure that the charge state of an ion in the crystal is nearly constant and depends little on its transverse energy. Another method was applied in planar channeling experiments [4], where the $E_\perp$ discrimination was obtained through a selection of particles with well-defined oscillation wavelengths. A third method was used in [5], where the $E_\perp$ discrimination was performed through a selection of the emergent charge state q_{out}. This method is particularly attractive when the initial charge state q_{in} of the ion is much lower than the equilibrium charge state, leading to a broad emergent charge state distribution $F_C(q_{out})$. The charge exchange processes are here dominated by the ionization of the projectile by the target electrons [electron impact ionization (EII)] with an efficiency that increases with the mean encountered electron density $\overline{\rho_e}(E_\perp)$ and hence with $E_\perp$. In particular, if $F_C(q_{out}=q_{in}) \ll 1$, selection of the frozen charge state $q_{out}=q_{in}$ can be used to select particles with very low $E_\perp$.

Our previous experiments at GANIL [5] are here extended to higher energies and heavier ions by using a

300-MeV/u uranium beam transmitted through a silicon crystal. The value of the Bohr parameter κ:

$$\kappa = \frac{2Z_1 v_o}{v} = 2\frac{Z_1}{137\beta} \tag{1}$$

corresponding to 300 MeV/u bare uranium ions is $\kappa \simeq 2$, i.e., greater than unity; a classical approach to calculation of energy transfers to target electrons is thus permitted [6].

The principal aims of the experiment presented in this paper are (i) to deduce EII cross sections from $F_C(q_{out})$ measurements for very high Z ions, for which simple perturbation treatments are questionable even at high velocities, (ii) to obtain experimental energy loss spectra as a function of q_{out} for comparison with semiclassical calculation of energy loss in channeling.

Our results on EII will be compared to various theoretical predictions and to other measurements, in particular to those of Claytor *et al*. [7], who also performed channeling measurements with uranium ions at similar energies, but using nearly stripped incident ions. More generally, an extended review of charge exchange processes for heavy ions in channeling was recently given by Krause and Datz [8]. In this review, the EII results obtained by channeling and by other methods such as electron beam ion trap (EBIT) are compared to theory.

In Sec. II we describe the experimental setup that allows charge state and energy analysis of the transmitted ions. In Sec. III we present our experimental data that include charge state distributions $F(q_{out})$ and energy loss spectra for given q_{out}, $g(\Delta E|q_{out})$. In Sec. IV we describe a simulation code that enables us to calculate both $F(q_{out})$ and $g(\Delta E|q_{out})$. The comparison of simulated and measured profiles is presented in Sec. V and the results are compared to theoretical calculations.

II. EXPERIMENT

We have used relativistic uranium ion beams [$Z_1=92$, $M_1=238$, $E_o=300$ MeV/u, i.e., $\beta=v/c=0.654$ and $\gamma=(1-\beta^2)^{-1/2}=1.32$] with $q_{in}=73$. The thickness $t=120$ μm of the silicon ($Z_2=14$) single crystal target along the $\langle 110\rangle$ axis was large enough to ensure a broad emergent charge state distribution $F_C(q_{out})$ (i.e., a good $E_\perp$ selection) and measurable energy loss distributions for each emergent charge state.

The experiment was performed at the heavy ion synchrotron SIS at GSI (Gesellschaft für Schwerionenforschung, Darmstadt), which provided a 300 MeV/u U^{73+} beam. The projectiles were injected into a high-resolution magnetic spectrometer (fragment separator FRS [9]), which consists of four ion optical stages each having one dipole magnet, five quadrupole magnets, and four hexapole magnets. The first two stages were used to prepare a beam of small angular divergence (see Fig. 1), which is a most important parameter in the experiment. The spot size on the silicon crystal was of the order of 10×15 mm^2. This large spot size was a necessary consequence of the optimization of the beam angular divergence. It had, however, minor influence on the experimental results as the rather thick silicon single crystal was large (20-mm diameter) and x-ray topography measurements

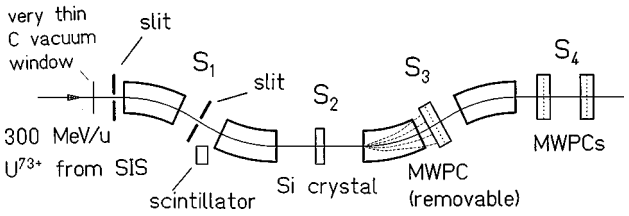

FIG. 1. Schematic layout of the experimental setup for channeling studies at the fragment separator FRS.

indicated negligible misalignment or mosaic spread. The beam intensity from SIS was typically $\approx 10^6$ ions per second. After charge and emittance selection by slits, it was $\approx 10^2$ ions per second on the crystal. The beam dose was calibrated and monitored using a scintillator outside the vacuum system, which measured secondary radiation due to the fraction of U ions hitting the slits.

The Si crystal target was mounted on a remotely controlled, high-resolution, three-axis goniometer designed for ultrahigh vacuum, placed at S_2, which could be moved with an accuracy of 0.01mrad. In the focal planes after the third and fourth stages of the FRS, the charge state distribution was measured using multiwire chambers [multiwire proportional counter (MWPC)] in S_3 and S_4. The wire chambers were used to determine the integral, position, and shape of the peak of a specific exit charge q_{out} state, giving information on the emergent charge state distribution, energy loss, and energy loss straggling. The correspondence between the position w (in mm) on the MWPC and the longitudinal momentum p of the particles, which depends on the measured rigidity Br (B, magnetic field; r, bending radius), is given by the dispersion D (in mm) via $\Delta p/p=\Delta w/D$ for our ion optical setting. In the FRS, one has $D_3=1380$ mm (for S_3) and $D_4=9530$ mm (for S_4). The charge state distributions were measured at S_3 and energy loss spectra at S_4. The variations Δp of momentum and variations ΔE of energy are related by $\Delta E/E=(1+1/\gamma)\Delta p/p=1.756\Delta p/p$, which gives $\Delta E_4=0.0553$ MeV/u and $\Delta E_3=0.38$ MeV/u for $\Delta w=1$ mm, respectively, in S_4 and S_3.

The alignment of the crystal for $\langle 110\rangle$ channeling was achieved either by maximizing the frozen charge state 73+ yield or by minimizing the 90+ emerging charge state yield (these yields were measured using a scintillator placed after the MWPC in S_4, in relation to the monitor scintillator near S_1). In reality, the observation of the frozen charge state yield gives here a much more precise alignment than given by the observation of the 90+ charge state yield (see Sec. III).

III. EXPERIMENTAL RESULTS

In Fig. 2 we present the measured yields of the emergent charge states $q_{out}=73$ (frozen) and $q_{out}=90$ as a function of the tilt angle φ_o between the beam direction and the $\langle 110\rangle$ axis. The angular distribution of the 73+ ions is very narrow, with a half width at half maximum of $\Psi_{1/2}^{73+}=0.11$ mrad. The observed angular scan for 90+ emergent ions is dominated by particles with high transverse energy, which were mostly ionized by close encounters with target nuclei (NII). The half width $\Psi_{1/2}=0.285$ mrad of the 90+

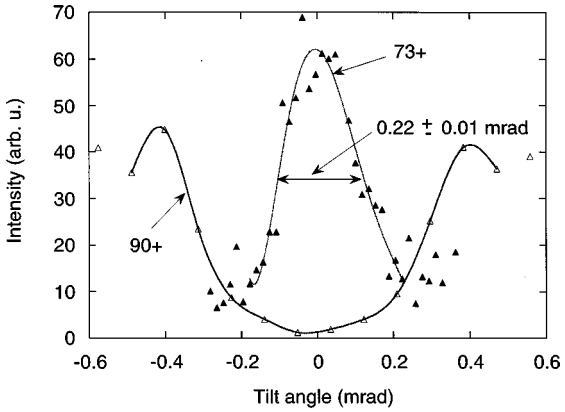

FIG. 2. Variations of the intensities of emergent charge states $q_{out}=q_{in}=73$ (closed triangles) and $q_{out}=90$ (open triangles) as a function of the angle φ_o between the beam and the $\langle 110\rangle$ axis of the Si crystal (lines through the points are drawn to guide the eye).

scan is thus, of course, larger than that of the 73+ scan. $\Psi_{1/2}$ is clearly related to the transverse energy $E_{\perp c}$ required to approach atomic strings at a distance of the order of ρ_{th}, the 2D rms of the thermal displacements of atoms perpendicular to the strings: $E\Psi_{1/2}^2 \simeq E_{\perp c} \simeq U_s(\rho)$, U_s being the string potential. The value of the Lindhard relativistic critical angle [10] $\psi_1=\sqrt{4Z_1Z_2e^2/pvd}$ is 0.39 mrad. Thus, we find a value $\Psi_{1/2}=0.73\psi_1$, somewhat smaller than extrapolated from numerical simulations [11] for a trial charge in silicon at room temperature, which gives $\Psi_{1/2}=0.85\psi_1$. An upper limit of the critical transverse energy $E_{\perp c}^{73+}$ to emerge in the frozen charge state $q_{out}=73$ is related to $E_{\perp c}$ by $E_{\perp c}^{73+}=(\Psi_{1/2}^{73+}/\Psi_{1/2})^2 E_{\perp c} \simeq 0.15E_{\perp c}$. In fact, $\Psi_{1/2}^{73+}$ is mainly determined by the beam angular divergence, as will be demonstrated in Secs. IV and V, and thus $E_{\perp c}^{73+}$ is certainly significantly smaller than this upper limit. The particles emerging with $q_{out}=73$ are very well-channeled ions, but $E_\perp$ selection through q_{out} is less accurate than that in Ref. [5]: the $q_{out}=73$ ions, which represent 3.8% of the emergent beam, are not all hyperchanneled (see Secs. IV and V). The minimum yield of the 90+ scan is $\simeq 5\%$. This is somewhat higher than the $\simeq 2\%$ yield obtained in Monte Carlo calculations by Barrett [11] or measured with MeV light ions on the same crystal and axis [12] for close encounter events. This may be explained, at least partially, by the fact that NII is not the only process for $q_{out}=90$ production; the binding energy of the L electrons of uranium is $B_L \simeq 20$ keV (it depends on the charge state) and the maximum energy transfer in a close encounter EII process is $\simeq Em_e/M_U=164$ keV. Hence, EII alone may produce 90+ uranium ions. Another important contribution to the 5% minimum yield comes from tails in the incoming beam angular distribution and to dechanneling (see Sec. IV).

Typical spectra measured with MWPCs at S_3 and S_4 are shown in Fig. 3. In Fig. 3(a) we show the charge state distribution $F_C(q_{out})$ at S_3 $(73 \leqslant q_{out} \leqslant 77)$ with the $q_{out}=73$ peak at the center. Figures 3(b) and 3(c) show the spectra for $q_{out}=73$ measured at S_4, respectively, with and without the silicon crystal. In Fig. 3(d), we show a spectrum for rather poorly channeled ions ($q_{out}=83$); the peak is broader than for $q_{out}=73$ reflecting larger energy loss fluctuations.

The measured emergent charge state distributions are given in Fig. 4, for $\langle 110\rangle$ aligned and random orientations. The distributions were obtained by measuring sequentially the intensity of three neighboring peaks for which the transmission from the Si crystal at S_2 to the MWPC at S_3 was equal to 1. In the random case, the narrow distribution $F_R(q_{out})$, centered around $q_{out}=90$, does not correspond to equilibrium: the target is not thick enough, considering the very small capture cross sections (MEC, REC) for the relativistic uranium ions studied. A tail towards low charge states, representing about 3% of the total beam is observed and we attribute this to planar channeling effects.

The aligned distribution $F_C(q_{out})$ is broad, as expected, reflecting the influence of $E_\perp$ on q_{out}. The upper region

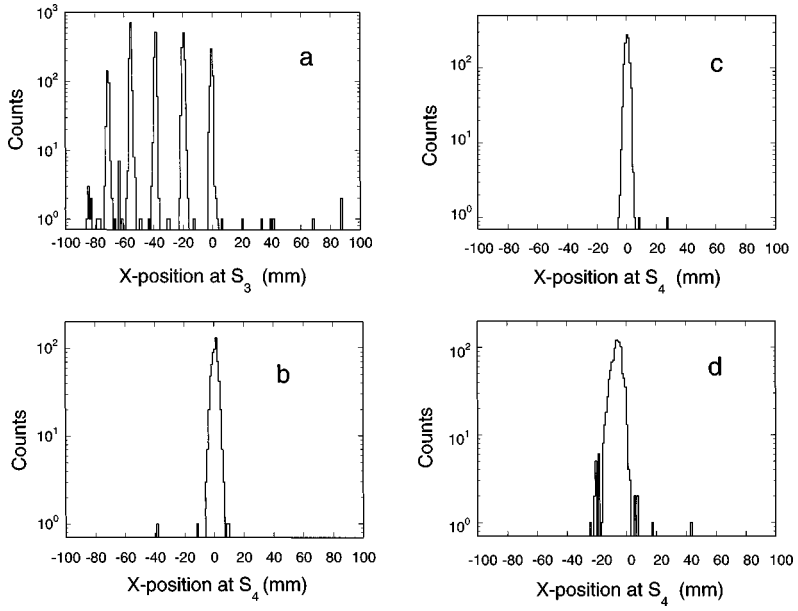

FIG. 3. Spectra measured with MWPCs at S_3 and S_4. (a) Charge state distribution at S_3 for $73 \leqslant q_{out} \leqslant 77$. (b) $q_{out}=q_{in}=73$ peak at S_4 with the crystal. (c) $q_{out}=q_{in}=73$ peak at S_4 for the direct beam. (d) $q_{out}=83$ peak at S_4.

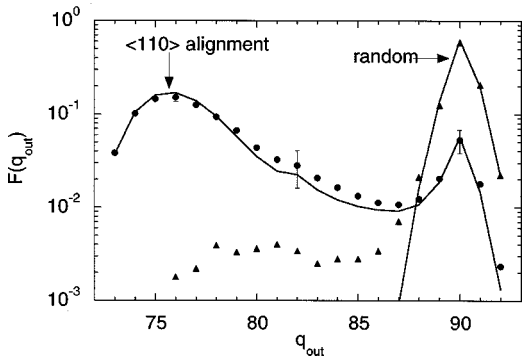

FIG. 4. Charge state distributions obtained for U^{73+} incident ions at 300-MeV/u after transmission through a 120-μm-thick Si crystal, for alignment along the $\langle 110\rangle$ direction [$F_C(q_{out})$, closed circles] and for random orientation [$F_R(q_{out})$, closed triangles]. The solid lines correspond to Monte Carlo calculations (see Sec. V).

($q_{out} \gtrsim 87$) of $F_C(q_{out})$ corresponds to very poorly channeled, nonchanneled, or dechanneled ions. This region contains about 10% of the distribution. Dechanneling alone cannot explain this rather high value, which is mainly attributed to the angular spread of the incoming beam (see Sec. IV).

In Fig. 5 the mean energy losses $\overline{\Delta E}(q_{out})$, measured with the MWPCs, for $\langle 110\rangle$ alignment, are plotted as a function of emergent charge state q_{out} together with random values measured for $q_{out}=89$ to 92. The increase of $\overline{\Delta E}$ with q_{out} arises (i) from the increase with q_{out} of the mean charge state $q_{av}(q_{out})$ of the particles inside the target. Here, $q_{av}(q_{out})$ is defined in such a way that the mean energy losses $\Delta E(q_{out})$ scales approximately as $q_{av}^2(q_{out})$ [see Sec. V B, Eq. (7)] (ii) from the increase of $E_\perp$ with q_{out} and the increase of stopping power S with $E_\perp$. Hence, the ratio $\overline{\Delta E}(q_{out})/q_{av}^2(q_{out})$ (also represented in Fig. 5), gives the influence of the transverse energy on mean energy loss. As in Ref. [5] for Xe ions, the mean energy loss in the random case is lower than the $\overline{\Delta E}(q_{out})$ value obtained under channeling conditions for very high transverse energies (here q_{out}

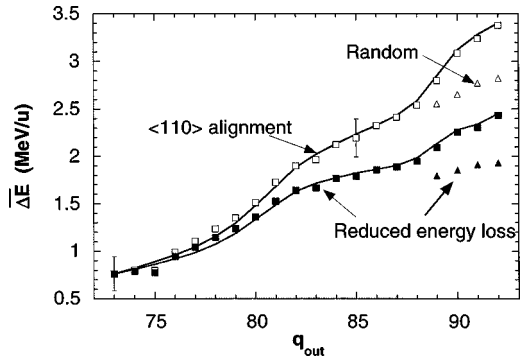

FIG. 5. Mean energy loss $\overline{\Delta E}(q_{out})$ measured with the wire chamber at S_3 as a function of emerging charge state q_{out} for U^{73+} incident ions transmitted in $\langle 110\rangle$ alignment conditions (open squares). The mean energy loss for random orientation and for $89 \leqslant q_{out} \leqslant 91$ are also shown (open triangles). The closed squares and triangles correspond to a reduced mean energy loss $\overline{\Delta E}(q_{out})q_{in}^2/q_{av}^2(q_{out})$ using the calculated mean charge state q_{av} in the target (see Sec. V). The solid lines are the results of the Monte Carlo calculations.

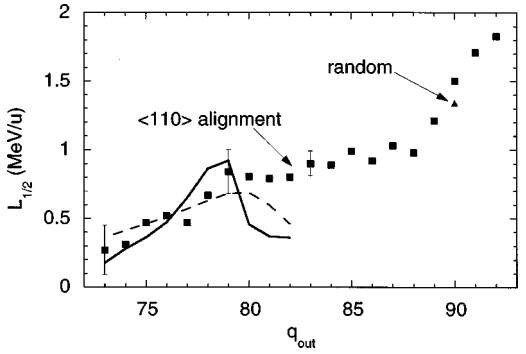

FIG. 6. FWHM of the energy-loss spectra $g(\Delta E|q_{out})$ as measured by the wire chamber at S_4, as a function of emergent charge state q_{out} for $\langle 110\rangle$ alignment (closed squares), and for random orientation ($q_{out}=90$, closed triangle). All of the data have been corrected for the resolution. The lines correspond to the Monte Carlo calculations: calculated FWHM (solid line), 2.355Ω (dotted line), where Ω^2 is the calculated variance.

$\geqslant 89$). This is a ''shoulder effect'': due to blocking by planes, particles with high transverse energy spend a larger part of their path close to the target nuclei than particles with random trajectories. The angular divergence of the beam being very small, even the measurement for the random incidence is not comparable to a measurement performed on an amorphous silicon target since channeling phenomena cannot be completely suppressed. This is obvious when one considers the shape of the energy loss spectra $g(\Delta E|q_{out})$. The full width at half maximum (FWHM) $L_{1/2}(q_{out})$ of the $g(\Delta E|q_{out})$ spectra is shown in Fig. 6. These FWHM values have been corrected for the distribution without the crystal (see Fig. 3), using a simple quadratic procedure. One observes an increase of the energy straggling with q_{out} for similar reasons as for $\overline{\Delta E}$. For the random measurement, the fluctuations are much larger than calculated by Monte Carlo simulations, whereas the mean value compares reasonably well with theory or compilation of experimental results (see Sec. V). In Fig. 7, we present the asymmetry figure $\mu^{1/3} = (\mu_3/\sigma^3)^{1/3}$ (μ is the skewness, μ_3 is the centered third order moment, and σ the standard deviation) of the energy loss spectra as measured with the MWPCs at S_4. Due to the

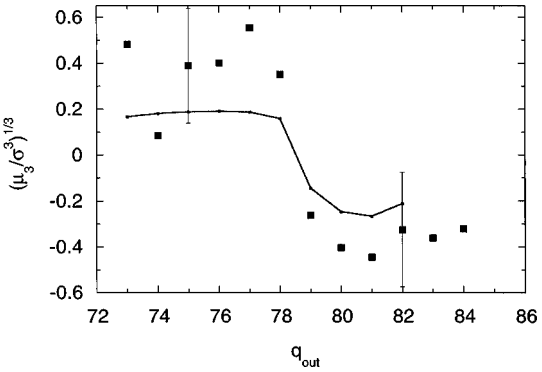

FIG. 7. Asymmetrical figure $\mu^{1/3}=\mu_3^{1/3}/\sigma$ of the energy loss spectra $g(\Delta E|q_{out})$ as a function of emergent charge state q_{out} in $\langle 110\rangle$ alignment. The points (closed squares) correspond to measurements made at the wire chamber in S_4. The Monte Carlo calculated $\mu^{1/3}$ is represented by the solid line.

very large uncertainties in the experimental results, only the qualitative behavior of $\mu^{1/3}$ should be considered. One observes clearly a sudden change in the sign of μ between $q_{out}=78$ ($\mu>0$, tail toward high energy losses) and $q_{out}=79$ ($\mu<0$, tail towards low energy losses). For $q_{out}<78$ one may consider $g(\Delta E|q_{out})$ as made up of a peak corresponding to well-channeled ions plus a tail corresponding to particles with higher $E_\perp$ whereas for $q_{out}>79$, $g(\Delta E|q_{out})$ consists of a peak corresponding to poorly channeled ions plus a tail corresponding to rather well-channeled ions, which have a finite probability to go out with $q_{out}>79$. This behavior was a useful guide in our simulations.

IV. MONTE CARLO SIMULATIONS

Simulations based on the calculation of ion flux distribution inside the crystal were used to calculate the emergent charge state distributions $F_C(q_{out})$ and energy loss spectra for a given exit charge state $g(\Delta E|q_{out})$. Less complex Monte Carlo simulations were used to simulate $F_R(q_{out})$ and $g(\Delta E|q_{out})$ corresponding to the random orientation. Similar simulations were already used and are described in Refs. [5] and [2]. We will only describe the most important features of the model.

For calculation time reasons, the simulations (for channeling or random cases) are not full Monte Carlo simulations, i.e., successive atomic collisions are not explicitly calculated. One consequence is that the behavior of ions with very high $E_\perp$ is not very well described because shoulder effects are not reproduced.

A. Calculation of the particle flux: Variations of the transverse energy with depth

An ion penetrating the crystal with energy E_o is given an entrance position $\vec{r}_{0\perp}$ (uniformly distributed in the transverse plane), and an entrance angle $\psi=\psi_o+\delta\psi$, which is distributed according to the beam angular distribution $h_b(\delta\psi)$ around the mean incident direction at angle ψ_0 to a $\langle 110\rangle$ axis. The precise knowledge of $h_b(\delta\psi)$ is crucial. Overall agreement between calculations and experimental results is found when $h_b(\delta\psi)$ is assumed to be the sum of a Gaussian with a 1D rms deviation of 0.075 mrad (i.e., $0.075\times\sqrt{2}=0.105$ mrad for the 2D distribution) and a much wider Gaussian distribution (1D rms 0.20 mrad), which contains 20% of the incident ions. Such a decomposition was necessary in order to reproduce the narrow angular scan $q_{out}=73$ of Fig. 2 and the emergent beam charge state distribution $F_C(q_{out})$ of Fig. 4, for $q_{out}\gtrsim 80$.

Particles are assumed to move in the continuum transverse potential U calculated in Ref. [5] for the $\langle 110\rangle$ axis of Si, corrected near the strings for thermal vibrations of the crystal atoms by using the single string potential of Ref. [13]. Statistical equilibrium is assumed for the transverse motion, and hence, a particle of given E_T has a uniform probability to be at any point in the accessible area of the transverse plane $A_\perp(E_\perp)$ [10]. This is true only sufficiently far from the crystal entrance since the incoming ions keep a ''phase memory'' at the beginning of their path [11] over a characteristic path length Λ. In our case, the crystal thickness ($t=120$ μm) is much greater than $\Lambda\approx 6$ μm and one may consider that statistical equilibrium prevails throughout the crystal (the Λ value was estimated from the Monte Carlo calculations of Barrett [11] and from the scaling $\lambda/2\approx d_n/\psi_c$ [14] for the oscillation length λ of close encounter yield due to neighboring strings at distance d_n). However, channeling with respect to planes introduces a more stable division of the transverse phase space of axially channeled particles into planar channeled and blocked trajectories, respectively [15]. This division is responsible for shoulder effects like the increase of the stopping power above the random value and the increase of energy loss fluctuations, which was not taken into account in the simulation.

Multiple scattering, which tends to increase the transverse energy, is taken into account. The changes in $E_\perp$ result from multiple scattering on target electrons and on screened target nuclei. A good estimate of the contribution of target electrons to multiple scattering can be obtained following Bonderup *et al.* [16], from the mean energy loss of these particles in the crystal. According to [16], the 2D variance $\delta\varphi_e^2$ of the angular distribution for a given path δx is

$$\overline{\delta\varphi_e^2}=\frac{m_e}{M_1}\frac{\overline{\delta E}_{close}}{E}, \tag{2}$$

where m_e is the electron mass and $\overline{\delta E}_{close}$ is the mean energy loss corresponding to close collisions with target electrons; roughly, $\overline{\delta E}_{close}=\frac{1}{2}\overline{\delta E}$. If δx is small enough to ensure a quasiconstant value of the transverse position $\vec{r}_\perp$ and of the angle $\vec{\varphi}$ of the trajectory with respect to the axis, the corresponding increase $\delta E_\perp$ in transverse energy is given by $E(\vec{\varphi}+\delta\vec{\varphi}_e)^2-E\varphi^2$, where $\delta\vec{\varphi}_e$ is a random deflection angle with variance given by Eq. (2). In what follows, the transverse energy will be systematically normalized to the unit charge and we then write:

$$q_{in}\delta E_\perp=E(\vec{\varphi}+\delta\vec{\varphi}_e)^2-E\varphi^2=2E\vec{\varphi}\cdot\delta\vec{\varphi}_e+E\,\delta\varphi_e^2. \tag{3}$$

This contribution to $\delta E_\perp$ by electron multiple scattering is taken into account in the Monte Carlo simulations.

Over the target thickness t, using the typical value $\overline{\Delta E}=1$ MeV/u for channeled ions (see Fig. 5), the contribution of the quadratic term in Eq. (3) is $E\overline{\Delta\varphi_e^2}/q_{in}=5$ eV. This can be compared to the critical transverse energy $E_{\perp c}=E\psi_1^2/q_{in}=150$ eV. The mean value of the nonquadratic term in Eq. 3 is null. Thus, this term contributes only to the transverse energy spread.

For the contribution to dechanneling of screened target nuclei we used the treatment proposed in Ref. [10] and developed in Ref. [17]. As for multiple scattering in a random medium, dechanneling by target nuclei for a given crystal and axial direction scales approximately as Z_1/E [10]. If, for example, one considers the experimental backscattering results of Ref. [12] for light ions along a $\langle 110\rangle$ axis of silicon, the reduced path length Z_1x/E for reaching a close encounter yield equal to 10% of the random yield is 2.7 μm MeV^{-1}, which gives $x\simeq 2$ mm in our case: dechanneling by target nuclei is thus small in our 0.12-mm-thick target.

When the transverse energy of a given ion exceeds a value $E_{\perp max}>E_{\perp c}$ we assume that the ion is no longer channeled (the code is in any case not able to describe particles

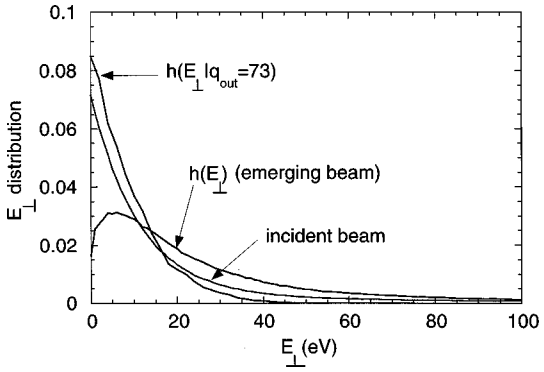

FIG. 8. Transverse energy distributions for the incident beam (characterized by its angular distribution, described by two Gaussians, see text), for the emerging beam and for emerging ions with $q_{out}=73$.

with very high $E_\perp$ correctly). If this occurs at depth x with a charge state q, it is necessary to calculate the charge state distribution of such an ion after traversing a random silicon target of thickness $t-x$ and with initial charge q: $F_R(q_{out}|q,t-x)$. This was done once, using the code ETACHA [18] for $73 \leqslant q \leqslant 92$ and various thicknesses x. Above a threshold value of 140 eV we found that the value of the parameter $E_\perp$ had no influence on the results. The curves presented in Sec. V were calculated with $E_{\perp max}=160$ eV; consequently, 3% of the beam was considered as random at $x=0$.

We show in Fig. 8 the transverse energy of the incoming beam, of the emerging beam, and of the 3.8% fraction of the emerging beam, which corresponds to $q_{out}=73$. This figure illustrates the influence of dechanneling on the overall beam. It also shows that this influence is very small for well-channeled particles emerging with $q_{out}=73$.

B. Charge exchange

Ionization and capture processes induced by target electrons (EII, REC) and by target nuclei (NII, MEC) are included in the simulations as well as excitation by electrons and nuclei, radiative and Auger decay. Ionization and excitation are assumed to be close encounter events with a probability proportional to the local electron or nucleus density. For a particle with a given $E_\perp$, the probability for target electron-induced processes is proportional to the mean electron density $\overline{\rho_e}(E_\perp)$ in $A(E_\perp)$. For nuclei, a cylindrical geometry around the strings was used (see [5]). The spatial extension of the ion electronic wave functions has nearly no effect on processes involving target electrons as the target electron density varies little at the scale of K,L,M orbital extension of uranium. For processes involving target nuclei (see [5]), a characteristic length is given by the 2D thermal vibrational amplitude $\rho=0.11$ Å at room temperature.

1. EII cross sections

The emergent charge state distribution $F_C(q_{out})$ is governed mainly by the EII processes; this means that rather significant uncertainties in NII, excitation and capture cross sections used in the simulations has a relatively minor influence on the determination of EII cross sections from the experiment. Conversely, it also means that the experiment is not appropriate to determine cross sections of other processes than EII. Although reliable values of NII, MEC, etc… cross sections are necessary in the simulations; some of these parameters may be varied over a reasonable range in order to improve the overall agreement with experimental results [in particular $F_R(q_{out})$] or to determine the precision that we may claim on the determined EII cross sections. For the EII cross sections themselves, we used theoretically calculated cross sections as a starting point and modified them until an optimum fit to the experiment was obtained.

For simplicity reasons, all cross sections were averaged over subshells in a given shell n. This is a fair approximation, as the main information that we reach is the EII cross section for M shell (see Sec. V A 1). In Sec. V A, the fitting values σ_{nfit}^{EII}, corresponding to EII in n shell will be compared to available theoretical predictions and to other experimental results. We now discuss the cross sections (other than EII) used in the Monte Carlo calculations.

2. NII cross sections

The NII cross sections were calculated in the plane wave Born approximation (PWBA) as described in Ref. [18], using screened hydrogenic wave functions for the initial and final states of atomic electrons. The calculated NII cross sections σ_n^{NII} per ion electron in shell n and per target nucleus are presented in Table I. They are two to three orders of magnitude higher than the corresponding σ_n^{EII} values. In particular, for the outer shells ($n>2$), the ratio $\sigma_n^{NII}/\sigma_n^{EII}$ is close to the square of the Si nuclear charge. Thus NII completely dominates for random ions, which shows that channeling is absolutely necessary to obtain information on σ_n^{EII}.

3. REC and MEC cross sections

REC cross sections for fully stripped ions were calculated according to the Bethe-Salpeter formula [19] and are given in Table I.

For MEC, we used two sets of cross sections. One set was calculated in the continuum distorted wave (CDW) approximation [20] using the code of Gayet [21]. The other set was calculated [22] in the simpler relativistic eikonal approximation [23,24]. The influence of the population of shells and subshells was taken into account by using the procedure suggested in [18], according to which the capture cross section to a given subshell is assumed to be simply proportional to the number of available vacancies.

4. Excitation cross sections

Cross sections σ_ν^{Exc} for excitation by target nuclei were calculated by Salin [25] for $n \leqslant 3$ using the PWBA approximation. Excitation cross sections for $n>4$ shells were extrapolated using a $1/n^3$ scaling. The σ_ν^{Exc} values are in the range 10^{-25} to 10^{-22} cm^2. The excitation cross sections by target electrons σ_e^{Exc} were calculated from the excitation cross section by target nuclei assuming a Z_2^2 scaling law.

5. Recombination processes

For an ion in a solid, intrashell mixing takes place and the mean life τ of an excited state is mainly governed by the

TABLE I. Theoretical cross sections averaged over subshells σ_{th} (in barns) (for EII cross sections, the index *Y* refers to Younger [33], *S* to Scofield [43], *F* to Fontes *et al.* [36], and *Kim* to calculations performed by [35] using the BED model of Kim and Rudd [34]). The cross sections σ_{fit} leading to the best overall agreement with the experimental results are expressed as a function of the σ_{th}.

Shell n	σ_{th}^{MEC}	σ_{th}^{REC}	σ_{th}^{NII}	σ_{th}^{EII}
1	17.8	71	600	0.6^{Kim}, 0.6^{Y}, 1.24^{F}
	$2s$:15.3			
2		14.8	5.9×10^{3}	18^{Kim}, 19^{Y}, 36^{S}
	$2p$:45.8			
	$3s$:5.5			
3	$3p$:16.6	4.3	1.6×10^{4}	76^{Kim}, 48^{Y}
	$3d$:27.7			
4	30	1.8	3.2×10^{4}	170^{Kim}
5	19	0.9	5.4×10^{4}	320^{Kim}
1–5	$\sigma_{fit}^{MEC}=0.5\sigma_{th}^{MEC}$	$\sigma_{fit}^{REC}=\sigma_{th}^{REC}$	$\sigma_{fit}^{NII}=1.3\times\sigma_{th}^{NII}$	$\sigma_{fit}^{EII}=(1.9\pm0.4)\times\sigma_{Kim}^{EII}$

fastest transitions, i.e., electric-dipole transitions [26]. We used the tables of Omidvar [27] that give the transition probabilities and branching ratios for electric-dipole transitions between levels of hydrogenlike atoms, using the $1/Z_1^4$ scaling (typical τ values are between 10^{-17} and 10^{-14} s). In the Monte Carlo code, Auger decay was taken into account for transitions from *M* to *L* shell only. The fluorescence yield (i.e., the probability of radiative decay) is $r_F=0.42$ [28] for a filled *M* shell (and at least a vacancy in *L* shell). For a given number m of *M* electrons ($1\leqslant m\leqslant 18$), $r_F(m)$ was calculated by assuming that the probability for Auger decay is proportional to $m(m-1)$ and the probability for radiative decay is proportional to m.

In our experiments, the dominant charge exchange process is ionization: capture and recombination processes have a relatively minor influence on the charge state distributions.

C. Energy loss

For the simulation of energy loss spectra, if one assumes statistical equilibrium, the only needed function is $S(E_\perp)$ that is an averaged value over the accessible transverse space $A(E_\perp)$ of the stopping power $S(\vec{r}_\perp)$ for an ion at position $\vec{r}_\perp$ in the transverse plane. We impose the asymptotic behavior at large $E_\perp$ to be

$$S(E_\perp)=S_R\left[1-\alpha\exp\left(-\frac{E_\perp d}{Z_2e^2}\right)\right], \tag{4}$$

where d is the interatomic distance along the $\langle 110\rangle$ axis and α an adjustable parameter; S_R is the stopping power for very large $E_\perp$, i.e., for random orientation. Expression (4) may be derived using the hypothesis of statistical equilibrium and the string potential $U_s(R)\simeq(Z_1Z_2e^2/Ed)\ln(1+3a^2/R^2)$ (where a is a screening radius) derived by Lindhard [10]. We assumed a q^2 dependence of $S(E_\perp)$ with the charge state ($73\leqslant q\leqslant 92$). This is reasonable, owing to the ion velocity and to the restricted spatial extension of the orbitals of uranium ions (see Sec. V B 2). Hence, one can write, for instance, $S(E_\perp,q)=S(E_\perp,q_{in})\times q_{in}^2/q^2$. In the following, we essentially use $S(E_\perp,q_{in})$, where $q_{in}=73$.

For channeled particles, the energy loss spectra are mainly determined by the shapes of the $E_\perp$ distribution $g(E_\perp)$ and of $S(E_\perp)$. At given $E_\perp$, one must consider fluctuations in energy loss, which arise from fluctuations in charge state q and from fluctuations in energy transfer in individual electronic collisions. The fluctuations in q are taken into account in the simulations through a q^2 dependence of the stopping power. In order to calculate the variance $\delta\Omega_T^2$ associated with the statistical variation in the energy transfer in successive collisions with electrons, we used recent theoretical [29] and experimental [30] results. At relativistic velocities, $\delta\Omega_T^2$ for a path length δx may be expressed as

$$\delta\Omega_T^2=4\pi q^2e^4\overline{\rho_e}\delta x\gamma^2X=\delta\Omega_B^2\gamma^2X, \tag{5}$$

where $\overline{\rho_e}$ is the mean electron density experienced, $\delta\Omega_B^2$ represents the nonrelativistic free-electron Bohr result [6], and X accounts for departure from the Rutherford scattering law. In our case, from [29] and [30] one finds $X\simeq 1.7$. An upper limit for Ω_T, which should correspond to the random case, is $\Omega_T=0.031$ MeV/u using $q=92$ and $\overline{\rho_e}=14$ electrons per atom.

All of these contributions to energy loss fluctuations are taken into account in the Monte Carlo calculation to construct the $g(\Delta E|q_{out})$ curves.

D. Simulations for random orientation

In order to calculate the charge state distributions $F_R(q_{out})$ and the energy loss spectra $g(\Delta E|q_{out})$ for random orientation, we used a special random code. In this program the ion history is described as a succession of binary collisions on homogeneous, randomly distributed atoms or valence electrons. There is, of course, no $E_\perp$ dependence in the random code. As in the channeling code, the individual interactions leading to energy loss are not described. However, charge-changing events are simulated and hence the main contribution to energy loss fluctuations is fully included.

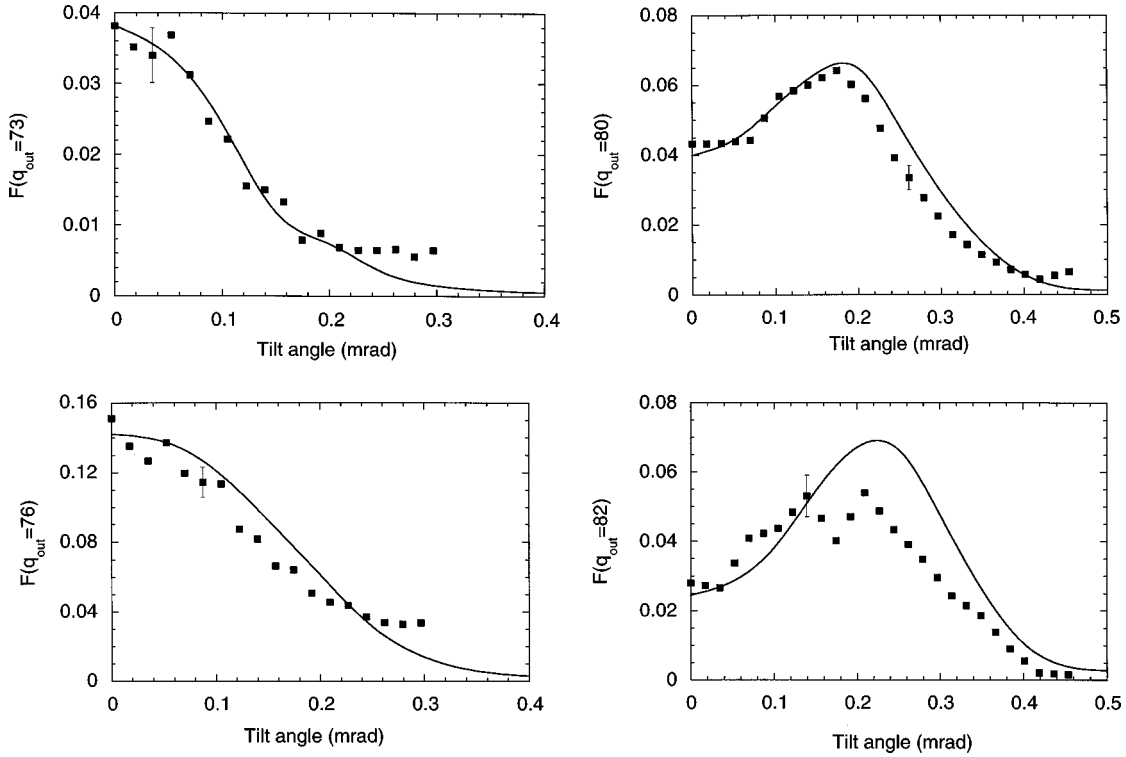

FIG. 9. Experimental angular scans (closed squares) of the fraction of emergent charge states $q_{out}=73,\ 76,\ 80,$ and 82 as a function of the angle between the beam and the $\langle 110\rangle$ axis of the Si crystal. The solid lines correspond to Monte Carlo calculations.

E. Fitting the experimental results

The experimental emergent charge state distributions $F_C(q_{out})$ and $F_R(q_{out})$, respectively, for $\langle 110\rangle$ channeling and for a random orientation, together with the energy loss spectra $g(\Delta E|q_{out})$, were fitted at the same time to ensure self-consistency. In order to limit the number of free parameters, we assumed in a first step that the ratios between theoretically calculated cross sections given in Table I corresponding to the different shells (for example, $\sigma_1^{EII}/\sigma_2^{EII}$) were reliable. In addition, excitation cross sections, REC cross sections (which play a minor role here), and decay probabilities were held fixed at their theoretical values. The adjustable parameters were then the scaling factor for the EII cross sections, the widths and proportion of the two Gaussians describing the incident beam angular divergence (see Sec. IV A) and the curve $S(E_\perp)$.

The Monte Carlo calculations were performed considering only 5 shells ($n\leqslant 5$): capture to higher excited states is nearly always followed immediately by ionization and these two events cancel.

V. RESULTS

A. Charge state distributions and EII cross sections

1. Charge states

Our best overall agreement leads to the solid lines in Fig. 4. The fitting of the random curve $F_R(q_{out})$ is sensitive mainly to NII and, to a lesser extent, to MEC. The fitting of the experimental $F_R(q_{out})$ does not lead to a unique set of cross sections. However, it appears that the calculated NII cross sections are not large enough to reproduce the large ($\simeq 55\%$) U^{90+} fraction and/or that calculated MEC cross sections are too large. The theoretically calculated MEC cross sections reported in Table I are those of [22] (eikonal approximation) for $n\leqslant 3$ and CDW cross sections [21] for $n>3$. These cross sections have a rather weak influence on the fitting of $F_C(q_{out})$ obtained for $\langle 110\rangle$ alignment. The solid curve in Fig. 4 was obtained with the fitting cross sections given in Table I.

The fit of $F_C(q_{out})$ is satisfactory. In particular, the region of $F_C(q_{out})$ with a quasirandom shape, which represents $\sim 10\%$ of the emergent ions, is well reproduced. The region $73\leqslant q_{out}\leqslant 80$ that corresponds to $\sim 75\%$ of the beam and for which $F_C(q_{out})$ is mainly due to EII in the uranium M shell is very well reproduced. The quality of the fit is highly sensitive to values of σ_3^{EII} introduced in the simulations. *The solid curve of Fig. 4 have been obtained with* $\sigma_{3fit}^{EII}=145b$ *per M shell electron.*

Experimental angular scans for four q_{out} values (73, 76, 80, 82) are shown in Fig. 9, together with the Monte Carlo calculated curves. It should be noted that, although we do not use a true channeling Monte Carlo code (statistical equilibrium is assumed), the calculated curves reproduce reasonably well the experimental data, considering that our main effort was devoted to the best channeled ions, i.e., $q_{out}=73$.

In order to gain more insight into the behavior of the channeled ions, we show in Figs. 10 and 11 various parameters given by the simulations, as a function of q_{out}: the mean transverse energy $\overline{E_\perp}(q_{out})$ (per unit charge), the mean sampled electron density $\rho_e(q_{out})$, the mean charge state in the target $q_{av}(q_{out})$, and the mean number of EII and NII events per ion, $N_{EII}(q_{out})$ and $N_{NII}(q_{out})$. The definition of q_{av} is based on the assumed q^2 scaling of the energy losses. If L_i represents the total path length travelled by an ion with

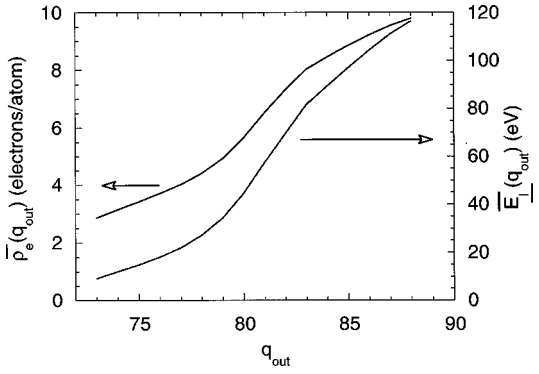

FIG. 10. Calculated mean transverse energy $\overline{E_\perp}(q_{out})$ (in eV, for unit charge) and mean sampled electronic density $\rho_e(q_{out})$ (in number of electrons per silicon atom) as a function of the exit charge state q_{out}. Calculations were carried out with the fitting parameters leading to the solid lines in Figs. 4 and 5.

transverse energy $E_\perp$ in charge state q_i, the mean energy loss in the target is

$$\overline{\Delta E}(E_\perp)=\overline{\sum_i q_i^2 S(E_\perp)L_i}=q_{av}^2 S(E_\perp)\times t. \tag{6}$$

We therefore define $q_{av}(q_{out})$ as

$$q_{av}^2(q_{out})=\left(\overline{\frac{1}{t}\sum_i L_i q_i^2}\right)_{q_{out}}. \tag{7}$$

$\overline{\Delta E}(q_{out})/q_{av}^2(q_{out})$ is the relevant parameter to relate the energy loss to $E_\perp$.

The $\overline{E_\perp}(q_{out})$ curve (Fig. 10) gives $\overline{E_\perp}(q_{out}=73)\simeq 9$ eV, whereas the map of the potential $U(\vec{r}_\perp)$ of Ref. [5] shows that ions are hyperchanneled for $U(\vec{r}_\perp)<2.2$ eV. The analysis of the distribution $h(E_\perp|q_{out}=73)$ shown in Fig. 8 demonstrates that this is the case only for 30% of the ions

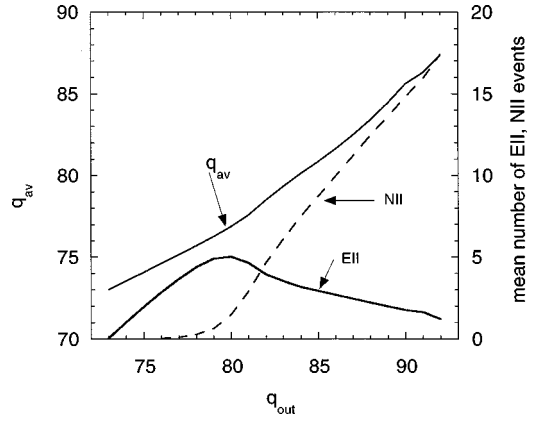

FIG. 11. Calculated mean charge state in the silicon crystal $q_{av}(q_{out})$ [as defined by Eq. (7)], mean number $N_{EII}(q_{out})$ of EII events per ion, and mean number $N_{NII}(q_{out})$ of NII events per ion, as a function of the exit charge state q_{out}. Calculations were carried out with the fitting parameters leading to the solid lines in Figs. 4 and 5.

emerging with $q_{out}=73$. The mean electron density $\overline{\rho_e}(q_{out}=73)$ sampled by $q_{out}=73$ ions is 2.8 electrons per atom (see Fig. 10).

EII events (see Fig. 11) dominate over NII events for $q_{out}\lesssim 81$, which confirms that our experiment allows a precise determination of the σ_3^{EII}(M shell) cross sections. However, due to the increasing role of NII, the sensitivity decreases rapidly for $q_{out}\gtrsim 82$. EII cross sections σ_2^{EII} for L shell electrons are not tested with precision and EII for K shell electrons (σ_1^{EII}) is not tested at all. The uncertainties in the NII cross sections are not the only source limiting the precision of the determination of σ_1^{EII} and σ_2^{EII} for high q_{out} (i.e., high $E_\perp$): $N_{NII}(q_{out})$ is very sensitive to the particle flux near the strings, which is not determined precisely enough in our simulations.

We now discuss our precision on the σ_3^{EII} cross sections determination and compare our results to other experimental results and theoretical predictions of the literature.

2. Precision on σ_3^{EII}

The precision on σ_3^{EII} relies on (i) the experimental uncertainties on $F_C(q_{out})$, (ii) the sensitivity of the fit to the σ_3^{EII} values, (iii) the various hypotheses introduced in the simulations to describe the particle flux, mainly the assumption on the beam angular divergence and the hypothesis of statistical equilibrium, and (iv) the precision on the knowledge of the electron density in the channel. When all parameters are fixed except the σ_3^{EII} value, the latter one can be varied by $\pm 10\%$ in order to remain within the error bars of $F_C(q_{out})$. The beam angular divergence is determined with precision when fitting the angular dependence of the various emergent charge states, particularly of the frozen charge state ($q_{out}=q_{in}=73$). Within the hypothesis of statistical equilibrium, the particle flux in the channels is mostly determined by the uniform distribution of the entrance impact parameter (the beam angular divergence and dechanneling effects introduce some modifications, which are taken into account in the simulations). We have seen above that the mean-free-path for the establishment of statistical equilibrium ($\sim 6\mu$m) is ~ 20 times smaller than t. The uncertainty on σ_3^{EII} introduced both by the small uncertainty on the incident beam angular divergence and by the hypothesis of statistical equilibrium is thus certainly small at the scale of 10%.

As for the mean electron density $\overline{\rho_e}(\vec{r}_\perp)$ in the transverse plane, we have compared predictions obtained by pseudopotential calculations [31] and values extracted by Scheringer [32] in order to fit the experimental x-ray form factors for silicon. The agreement between the two density maps is very good for $\vec{r}_\perp$ such that $U(\vec{r}_\perp)>10$ eV. However, discrepancies exist near the channel center, which never exceed 30%. When considering the available transverse space for frozen $73+$ ions, the overall discrepancy between the sampled electron density $\overline{\rho_e}(E_\perp;q_{out}=73)$ obtained from [31] and [32] does not exceed 15%. This is thus also the typical precision on σ_3^{EII} specifically related to the uncertainties on $\overline{\rho_e}(\vec{r}_\perp)$. In Sec. V B 2, we show that the agreement between the extrapolated stopping power at the channel center and theoretical estimates is better than 10%. This agreement is a good check of the theoretical predictions on energy loss, but it also

indicates that the $\overline{\rho_e}(\vec{r}_\perp)$ values that we introduced in our simulations are reliable, which comfort our confidence on the σ_3^{EII} determination. Finally, considering all sources of uncertainties, we conclude that the overall precision on the values of σ_3^{EII} that we determine is $\sim 25\%$.

3. Comparison with EII calculations

Very few theoretical calculations of σ_3^{EII} are available in our experimental situation. The kinetic energy E_e of the target electrons in the ion rest frame ($E_e = 164$ eV) is large compared to the mean M-shell binding energy of uranium ($B_M \simeq 10.3$ keV), a situation favorable for a perturbation treatment. However, the presence of many electrons and the very high nucleus charge introduce difficulties, which may lead to rather approximate results. A value can be extrapolated from Younger [33] (nonrelativistic distorted-wave Born exchange approximation, sodiumlike ions), giving $\sigma_{3Y}^{EII} = 45$ b per M-shell electron. This estimate is ~ 3 times smaller than the value σ_{3fit}^{EII} extracted from our measurements. We have also compared our results to the prediction for σ_{nKim}^{EII} of Kim and Rudd [34], which combines the binary encounter approximation with the dipole interaction of the Bethe theory [binary encounter dipole approximation (BED)]. Calculations based on this model were performed [35] using a relativistic Hartree-Fock Slater description of the uranium ion. The result is $\sigma_{3_{BED}}^{EII} = 76$ b per M-shell electron, i.e., ~ 1.9 times smaller than σ_{3fit}^{EII}. This is a fair agreement considering the degree of approximation of the BED model for very heavy ions with many electrons. Relativistic distorted-wave EII calculations have recently been published by Fontes *et al.* [36] for the ionization of K-shell H-like and He-like uranium ions, for an electron energy ($E_e = 198$ keV) close to ours. These calculations show that when the generalized Breit interaction is taken into account [distorted wave Breit approximation (DWB)], the cross section $\sigma_{1_{FBreit}}^{EII}$ calculated is ~ 1.5 times higher than predicted when only taking into account the Coulomb interaction beween bound and free electrons. $\sigma_{1_{FBreit}}^{EII}$ is found $\sim$ twice higher than the value σ_{1Y}^{EII} obtained from Younger [37]. Assuming that the ratio $\sigma_Y^{EII}/\sigma_{FBreit}^{EII}$ is also $\simeq 0.5$ for L or M shells, we would expect $\sigma_{3_{FBreit}}^{EII}$ to be ~ 1.5 times smaller than our measured value. Given the uncertainty of 25% in our measurement, this may appear as a reasonable agreement, even though the extrapolation may not be fully valid.

4. Comparison with other EII measurements

We have not found experimental information on σ_3^{EII} measurements for very heavy ions. The data available concern σ_1^{EII} and σ_{2s}^{EII}. For these cross sections, results were obtained for highly stripped uranium ions, with E_e rather close to ours. In electron beam ion trap (EBIT) experiments, Marrs *et al.* [38] find σ_{1s}^{EII} and σ_{2s}^{EII} in very good agreement with the values of $\sigma_{1sFBreit}^{EII}$ and $\sigma_{2sFBreit}^{EII}$ calculated by Fontes *et al* [36]. The EII cross sections for K and L-shell ionization of uranium ions with $E_e = 222$ keV have been measured by Claytor *et al.* [7] in a pioneer channeling experiment in silicon, using 405 MeV/u uranium ions with charge state $88 \leqslant q_{in} \leqslant 92$. The authors of Ref. [7] take benefit in the fact that channeled ions have charge exchange only through EII and REC. Assuming the REC cross section to be known, the analysis of $F_R(q_{out})$ and $F_C(q_{out})$ provides the fraction of channeled ions, the mean electron density $\overline{\rho_e}$ sampled by channeled ions and ultimately σ_1^{EII} and σ_{2s}^{EII}. The result for K-shell ionization is rather surprising: the authors find a value $\sigma_1^{EII} \sim 3$ times larger than predicted by Fontes *et al.* and ~ 6 times higher than predicted by Younger [37]. However, the agreement becomes fair for L-shell ionization, for which the experimental value is ~ 1.5 greater than predicted by Younger [33,37]. The surprisingly high values found for σ_1^{EII} in Ref. [7] may be due to the fact that for 90^+ and 91^+ incident ions, there is a strong overlap between $F_C(q_{out})$ and $F_R(q_{out})$ and thus that NII events may interfere when estimating σ_1^{EII}. The main difference between the experiment [7] and ours is related to the fact that in our case the incident ion charge is much farther from the equilibrium charge state reached in a random Si medium. We are thus able to discriminate between the available accessible areas experienced by ions emerging with different q_{out}. Consequently, in our case the mean electron density sensed is a function of q_{out} [for example, $\overline{\rho_e}(q_{out}=74) = 3.1$ electron per atom and $\overline{\rho_e}(q_{out}=80) = 5.6$ electron per atom, see Fig. 10]. Moreover, the σ_{3fit}^{EII} value we obtain must be consistent not only with the measured broad distribution $F_C(q_{out})$ but also with the energy loss spectra for each q_{out}. On the contrary, in Ref. [7] a single mean electron density is considered, corresponding to an average over all channeled ions, whatever q_{out} is. As the beam angular divergence was not small at the scale of $\Psi_{1/2}$ and as moreover some crystal bending effects were observed, the mean electron density was rather high, $\overline{\rho_e} = 6.2$ electrons per atom.

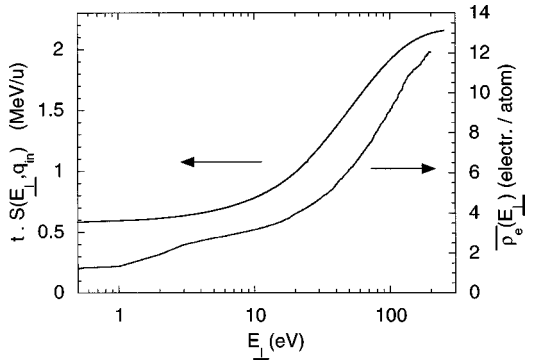

FIG. 12. Calculated curve for the mean energy loss $S(E_\perp, q_{in})t$ as a function of $E_\perp$ (in eV, for a unit charge), for an ion of charge state q_{in} in $\langle 110 \rangle$ alignment. The mean electron density $\overline{\rho_e}(E_\perp)$ sampled by ions of given transverse energy $E_\perp$ is also shown.

B. Energy loss

1. Fitting the experimental results

If one keeps constant all the adjustable parameters used to fit the experimental results for charge states, the energy loss results can be fitted using various $S(E_\perp)$ trial curves. A good overall agreement between experiment and calculation is obtained with the the mean energy loss curve $tS(E_\perp, q_{in})$ of Fig. 12. In this figure we show also the mean electronic

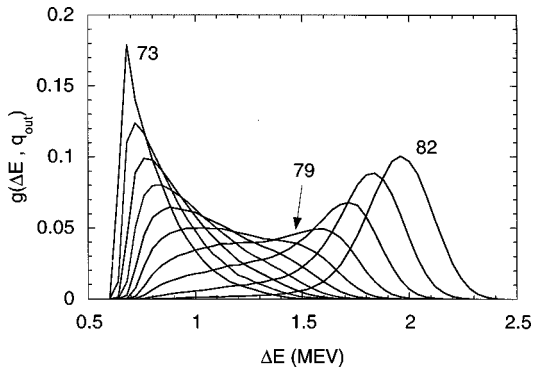

FIG. 13. Energy-loss spectra $g(\Delta E|q_{out})$ obtained by Monte Carlo simulations for $73 \leqslant q_{out} \leqslant 82$.

density $\overline{\rho_e}(E_\perp)$ sampled by ions of transverse energy $E_\perp$. Energy loss spectra $g(\Delta E|q_{out})$ were calculated using the $tS(E_\perp, q_{in})$ curve of Fig. 12 and the $E_\perp$ distribution experienced in the crystal by ions emerging with q_{out}. These calculated spectra are shown in Fig. 13 for $73 \leqslant q_{out} \leqslant 82$, i.e., in a transverse energy domain ($E_\perp \lesssim 70$ eV) for which the calculation is expected to give reliable results. These curves are, in most cases, asymmetrical and change rapidly in mean value and width from one charge state to the next. A broad $g(\Delta E|q_{out})$ curve corresponds to a broad transverse energy distribution $h(E_\perp|q_{out})$ and to a large slope of the $S(E_\perp)$ curve in the $E_\perp$ region covered by this distribution.

The mean values $\overline{\Delta E}(q_{out})$ of the calculated $g(\Delta E|q_{out})$ curves (the mean energy losses) are compared to the measurements in Fig. 5 (solid line). The calculated FWHM $L_{1/2}$ values of the $h(E_\perp|q_{out})$ curves are compared to the measured values in Fig. 6. The agreement is satisfactory for $q_{out} < 79$. On the contrary, for high q_{out}, the calculated values of $L_{1/2}$ (not shown) are much smaller than the measured ones. This is also the case for the calculated values of $L_{1/2}$ associated with random energy loss. One obtains $(L_{1/2}^{rand})_{calc} = 0.129$ MeV/u, a value nearly independent of q_{out} and slightly dominated by the charge state fluctuations. This Monte Carlo FWHM is calculated with a reasonable precision but is however ~ 10 times smaller than the experimental value $(L_{1/2}^{rand})_{exp} = 1.3$ MeV/u. Such a result is rather intriguing even if the concept of random orientation in a single crystal is rather questionable.

The asymmetry figure $\mu^{1/3} = (\mu_3)^{1/3}/\sigma$ is presented in Fig. 7. We did not measure reliable absolute values of μ. Nevertheless, the simulations reproduce the qualitative behavior of μ, i.e., a sudden change in the sign of μ between $q_{out} = 78$ and $q_{out} = 79$, with slower variations on either side. The $78 \leqslant q_{out} \leqslant 79$ region corresponds to the broadest calculated $g(\Delta E|q_{out})$; $L_{1/2}$ is of the order of 70% of the mean energy loss [broad $h(E_\perp|q_{out})$ and large slope for $S(E_\perp)$].

The most reliable information that we obtain on stopping is the mean energy loss, particularly for ions with very small $E_\perp$. The measured value $\overline{\Delta E}(q_{out} = 73) \simeq 0.76$ MeV/u together with the slope of the fitting curve $S(E_\perp)$ determined from low q_{out} mean losses ($tdS/dE_\perp \simeq 20$ keV/u per eV) give the extrapolated value $tS(E_\perp = 0) \simeq 0.57$ MeV/u. At low $E_\perp$ (see Fig. 12), the variation of $S(E_\perp)$ with $E_\perp$ is slower than the variation of the mean sampled electronic density, but however the $S(E_\perp)$ variation is faster than for 27 MeV/u Xe ions (see Ref. [5]). Interpreting this difference is not easy: it depends on the relative contributions of small and large impact parameters to energy loss due to valence and core target electrons. The results of energy loss for well-channeled uranium ions are analyzed in some detail in Sec. V B 2.

2. Theoretical survey. Comparison to experimental results

In this section, our aim is to estimate the theoretical energy loss $\overline{\Delta E}(E_\perp = 0)$ at the center of the channel and to compare it to the experimental extrapolated value.

The case of 300-MeV/u U^{73+} ions is rather complex for the following reasons: (i) the velocity is relativistic ($\beta = 0.654$). (ii) The Bohr parameter κ is larger than 1 ($\kappa = 2$ for bare uranium), which is not usually the case for high velocities. (iii) The ion velocity is much larger than orbital velocities of the target electrons, which would usually imply a perturbation treatment.

(a) Mean energy loss to valence electrons. Let us first consider the mean energy loss $\overline{\Delta E}_{val}^{max}$ for a uniform flux of point charge particles (i.e., a random beam). For relativistic ions with $\kappa > 1$, $\overline{\Delta E}_{val}^{max}$ may be expressed as

$$\overline{\Delta E}_{val}^{max} = t \frac{4\pi q^2 e^4}{m_e v^2} \overline{\rho}_{val} [L_B^{val} + \ln(\gamma^2) - \beta^2 + \Delta_{LS}(\gamma)], \tag{8}$$

where $\overline{\rho}_{val}$ is the mean valence electron density (4 electrons per silicon atom). L_B^{val} is a logarithmic term which may be expressed as

$$L_B^{val} \simeq \ln\left(\frac{p_{\max}}{p_{\min}}\right) = \ln\left(\frac{1.123 v/\omega}{b/2}\right) = \ln\left(\frac{1.123}{\kappa} \frac{2 m_e v^2}{\hbar \omega}\right). \tag{9}$$

In Eq. (9), p_{max} and p_{min} are effective integration limits over the impact parameter p. The higher limit, $p_{\max} = 1.123 v/\omega$ is an adiabatic cutoff [6]. A simple estimate of ω is given by the plasma frequency $\omega_p = (4\pi \overline{\rho}_{val} e^2/m_e)^{1/2}$ which gives $\hbar\omega_p = 16.6$ eV. For 300 MeV/u U ions, one finds $p_{\max} = 8.73$ nm, i.e., a very large value on the atomic scale. The effective lower limit $p_{min} = b/2$ is given by the collision diameter:

$$b = \frac{2qe^2}{m_e v^2}. \tag{10}$$

The second and third term in the bracket of Eq. (8) represent the usual relativistic correction of the first-order quantum perturbation theory.

$\Delta L_{LS}(\gamma)$ is a correction term representing the deviation to the perturbation theory, which has been recently calculated by Lindhard and Sørensen [29] (see Fig. 1 of this reference). The predicted value $\Delta L_{LS}(\gamma)$ has been confirmed experimentally by Datz *et al.* [39] for ultrarelativistic Pb ions. In our case, ΔL_{LS} represents $+3\%$ of the overall bracket term in Eq. (8). Then, with $q = 73$, Eq. (8) gives $\overline{\Delta E}_{val}^{max} = 155.5$ MeV $= A \times 0.654$ MeV/u. This value, calculated

with $\overline{\rho}_{val}=4$ electrons/atom, is an upper limit for the energy loss to the target valence electrons of channeled U^{73+} (it corresponds to the random case).

(b) Mean energy loss at $E_\perp=0$: contribution of valence and core electrons. A precise determination of the mean energy loss $\overline{\Delta E}_{val}$ for a channeled beam may be reached by an impact parameter approach (which is possible for $\kappa>1$) and by integration in the channel using local electronic densities $\overline{\rho_e}(\vec{r}_\perp)$ (here, averaging on ρ_e is performed along the $\langle 110\rangle$ direction only). For symmetry reasons (cylindrical geometry may be used), this type of calculation is tractable for ion trajectories just in the middle of the channel. This approach, leading to a calculated value based on the variations of ρ_{val} with the distance from the channel center, was already used in [5] and is presented in detail in Ref. [3]. Using Eq. (23) of [3], one finds

$$\overline{\Delta E}_{val}(q_{out}=73,E_\perp=0)=0.415 \text{ MeV/u}. \tag{11}$$

This value is 37% smaller than $\overline{\Delta E}_{val}^{max}$ and is to be compared with the overall mean energy loss 0.57 MeV/u extrapolated with the help of simulations from the experimental result.

This comparison indicates that, as pointed out in [3], and in contrast to the case of MeV light ions, the contribution of Si core electrons to the energy loss of very well-channeled swift heavy ions is not negligible. Whereas the adiabatic cutoff for *K*-shell Si electrons is small ($p_{ad}^K=0.40$ Å, using $\hbar\omega_K=3.2$ keV) as compared to the distance p_{str} between the channel center and the neighboring strings (of the order of 2 Å), this is not the case for *L* electrons: $p_{ad}^L=4.16$ Å , using $\hbar\omega_L=0.31$ keV. The adiabaticity parameter for ions at the channel center in their interaction with *L* target electrons is $\xi=p_{str}/p_{ad}^L\simeq 0.5$. Using Eqs. (19) and (20) of Ref. [3], one finds, using a similar notation, $R(\xi)=0.9$, $\overline{\Delta E^L}_{free}=0.17$ MeV/u, i.e., a mean energy loss to *L* electrons $\overline{\Delta E^L}=R(\xi)\overline{\Delta E^L}_{free}=0.15$ MeV/u, which represents 36% of the mean energy loss to valence electrons. The theoretical mean energy loss for U^{73+} ions channeled with zero transverse energy is then

$$\overline{\Delta E}(q_{out}=73,E_\perp=0)=\overline{\Delta E^L}+\overline{\Delta E}_{val}=0.565 \text{ MeV/u}. \tag{12}$$

This theoretical result is in excellent agreement with the experimental extrapolated result, 0.57 MeV/u at $E_\perp=0$. Such a good agreement is somewhat surprising when considering both the experimental uncertainties and the theoretical approximations. In particular, the above calculations assume the ion to be a point charge (perfect screening), which is not such a good approximation in the case of U^{73+} ions. The spatial extension of *M*-shell orbitals of uranium is of the order of $r_M=0.07$ Å . Using simple electrostatics and the shell electron density, one can estimate the effective charge q_{eff} seen by a target electron in an electron-U^{73+} interaction with an impact parameter *p*: qualitatively, $q_{eff}(p>r_M)=73$ and $q_{eff}(p<r_M)>73$. The influence of the variations of q_{eff} on mean energy loss was crudely calculated classically, by integration over impact parameters ($p_{min}<p<p_{max}$), which leads to an increase of 5% of the loss, i.e., $\overline{\Delta E}(q_{out}=73,E_\perp=0)=0.595$ MeV/u. Even with this correction, the agreement with the experimental result is still fair (4% discrepancy, of the order of the precision of the measurements). Hence, the semiclassical approach presented above is appropriate to describe energy loss processes for hyperchanneled 300-MeV/u U^{73+} ions.

Finally, it is interesting to note that one may associate with Eq. (11) an effective valence density $\rho_{eff}^{val}=4\overline{\Delta E}_{val}/\overline{\Delta E}_{val}^{\max}=2.54$ electron per atom. This value is much larger than the mean electronic density at the center of the channel (one electron per atom), which shows that the contribution of distant collisions is very important. When considering the $\rho_e^{val}(\vec{r}_\perp)$ and $U(\vec{r}_\perp)$ maps [5], one may anticipate that for $E_\perp\gtrsim 10$ eV the loss to valence electrons is independent of $E_\perp$ (and equal to $\overline{\Delta E}_{val}^{\max}$) and thus that the slope of $S(E_\perp)$ Fig. (12), which is determined with precision in this experiment, is entirely due to the contribution of core electrons.

3. Random energy loss

For random orientation, one may calculate the mean energy loss using a similar semiclassical approach (Eq. 8). The electron density is now $\overline{\rho}_e=Z_{Si}=14$ electrons per atom and the frequency ω in Eq. (9) is now an averaged value ($\hbar\omega=174$ eV) with weighting factors given by the dipole oscillator strengths of Ref. [40]. We obtain $\overline{\Delta E}_{R_{th}}(q=90)=2.605$ MeV/u. For comparison, the tabulation of Ziegler [41] gives $\overline{\Delta E}_R=2.87$ MeV/u. The experimentally determined values $\overline{\Delta E}_{R_{\exp}}(q_{out}=89)=2.5$ MeV/u and $\overline{\Delta E}_{R_{\exp}}(q_{out}=90)=2.65$ MeV/u are not to be compared directly to the above prediction, obtained for $q=90$. For the incident $q_{in}=73$ beam and the thickness $t=120$ μm, the mean charge state q_{av} throughout the target [see Eq. (7)] is somewhat smaller than q_{out}. Using the Monte Carlo random code, we calculated q_{av} as a function of q_{out} and obtained $q_{av}(q_{out}=89)=87.05$ and $q_{av}(q_{out}=90)=87.85$. Using these values, the theoretical mean energy losses are now $\overline{\Delta E}_{R_{th}}(q_{out}=89)=2.43$ MeV/u and $\overline{\Delta E}_{R_{th}}(q_{out}=90)=2.48$ MeV/u, which are smaller, but close to the experimental results. However, even in the measurements performed in the ''random'' orientation, channeling effects clearly appear as demonstrated by the very large width of the energy loss spectra. These effects may seriously affect the experimental mean energy loss value. It is hence hardly possible to confirm the general trend observed in Ref. [42] for relativistic very heavy ions, with $\kappa<1$, i.e., a stopping value $\sim$ 10% higher than given by the Born approximation.

Assuming a q^2 law, the random energy loss for $q=73$ would be $2.65\times(73/87.85)^2=1.83$ MeV/u. The mean energy loss $\overline{\Delta E}_c(73)$ for channeled $q=73$ ions, normalized to the random energy loss is then $\overline{\Delta E}_c(73)/\overline{\Delta E}_R(73)=0.76/1.83=0.41$. This ratio may appear rather high if directly compared to the mean encountered electronic density $\overline{\rho}_e(q=73)=2.8$ electron per atom normalized to the overall electronic density, i.e., $2.8/Z_2=0.2$. It illustrates again the large contribution of distant collisions.

VI. SUMMARY AND CONCLUSIONS

We have performed a channeling experiment with 300-MeV/u U^{73+} ions on a silicon single crystal. The angu-

lar divergence of the beam in the fragment separator FRS at GSI (Darmstadt), which was checked in our Monte Carlo simulations, was small as compared to the channeling critical angle.

The incoming charge state ($q_{in}=73$) of the beam was chosen to be much lower than the equilibrium charge state in silicon in order to discriminate among particles of various transverse energies by selecting emergent charge states. In particular, the ions transmitted in a frozen charge state ($q_{out}=q_{in}$) have travelled through the crystal with small transverse energies (1/15 of the critical transverse energy). The measurement of the energy loss of these ions was used to study the contribution of the various electron shells of silicon. The experimental results are consistent with the semiclassical model of Bohr, which predicts a large contribution (25%) of energy loss to silicon *L*-shell electrons, for ions with zero transverse energy. The main features of the variations of the width and asymmetry of the energy loss spectra are well reproduced by Monte Carlo simulations for well-channeled ions. In particular, the energy loss spectra for ions with $q=78$ and 79 are very broad (FWHM values of the order of 70% of the mean energy loss) and have opposite asymmetries.

The good agreement between measured and predicted energy losses for well-channeled ions provides a strong indication that the mean electron densities $\overline{\rho_e}(E_\perp)$ used in the Monte Carlo code are reliable with a precision better than 10%. These densities enter directly in the extraction of the EII cross sections from the experimental results. We have thus been able to obtain reliable quantitative information on the dominant charge exchange process for well-channeled ions. The simulations show that our experiment tests mainly and precisely the *M*-shell ionization of the uranium ions. Fitting the measured experimental emergent charge state distribution gives σ_3^{EII} cross sections that are twice larger than the values calculated using the binary encounter dipole model. Recent calculations of σ_1^{EII} using the relativistic distorted wave approximation with Breit corrections provide very good agreement with precise experimental EII cross section measured by EBIT for uranium, using electrons with energy E_e close to ours. It would be interesting to compare our results with an extension of such calculations to the *M*-shell of heavy ions with many electrons.

ACKNOWLEDGMENTS

The authors are very grateful to P. Indelicato, C. de Billy, A. Salin, C. Stefan, R. Gayet, and J.P. Rozet for their calculations of ionization, excitation, and capture cross sections, and for fruitful discussions. We thank the GSI facility operating staff, and K.H. Behr, A. Brünle, and K. Burkhard for technical assistance. This work was partially supported by the IN_2P_3-GSI collaboration agreement and the CNRS under GDR 86. We also acknowledge NATO support through Collaboration Grant No. CRG 901025.

[1] B.R. Appleton, C. Erginsoy, and W.M. Gibson, Phys. Rev. **161**, 330 (1967).
[2] S. Andriamonje, M. Chevallier, C. Cohen, N. Cue, D. Dauvergne, J. Dural, F. Fujimoto, R. Kirsch, A. L'Hoir, J.-C. Poizat, Y. Quéré, J. Remillieux, C. Röhl, H. Rothard, J.P. Rozet, D. Schmaus, M. Toulemonde, and D. Vernhet, Phys. Rev. A **54**, 1404 (1996) .
[3] J.U. Andersen, J. Chevallier, G.C. Ball, W.G. Davies, J.S. Forster, J.S. Geiger, J.A. Davies, H. Geissel, and E.P. Kanter, Phys. Rev. A **54**, 624 (1996).
[4] B.R. Appleton, R.H. Ritchie, J.A. Biggersaff, T.S. Noggle, S. Datz, C.D. Moak, H. Verbeek, and V.N. Neelavathi, Phys. Rev. B **19**, 4347 (1979).
[5] A. L'Hoir, S. Andriamonje, R. Anne, N.V. De Castro Faria, M. Chevallier, C. Cohen, J. Dural, M.J. Gaillard, R. Genre, M. Hage-Ali, R. Kirsch, B. Farizon-Mazuy, J. Mory, J. Moulin, J.C. Poizat, Y. Quéré, J. Remillieux, D. Schmaus, and M. Toulemonde, Nucl. Instrum. Methods Phys. Res. B **48**, 45 (1990).
[6] N. Bohr, K. Dan. Vidensk. Selsk. Mat. Fys. Medd. **27**, No. 15 (1948).
[7] N. Claytor, B. Feinberg, H. Gould, C.E. Bemis, J. Gomez del Campo, C.A. Ludemann, and C.R. Vane, Phys. Rev. Lett. **61**, 2081 (1988).
[8] H.F. Krause and S. Datz, in *Advances in Atomic, Molecular, and Optical Physics*, edited by B. Bederson and H. Walther (Academic, New York, 1996), Vol. 37, p. 139.
[9] H. Geissel *et al.*, Nucl. Instrum. Methods Phys. Res. B **70**, 279 (1992).
[10] J. Lindhard, Mat. Fys. Medd. K. Dan. Vidensk. Selsk. **34**, No. 14 (1965).
[11] J.H. Barrett, Phys. Rev. B **3**, 1527 (1971).
[12] D. Schmaus, F. Abel, M. Bruneaux, C. Cohen, A. L'Hoir, G. Della Mea, A.V. Drigo, S. Lo Russo, and G.G. Bentini, Phys. Rev. B **19**, 5581 (1979).
[13] A. Doyle and I. Turner, Acta Crystallogr., Sect. A: Cryst. Phys., Diffr., Theor. Gen. Crystallogr. **24**, 390 (1968).
[14] *Channeling, Theory, Observation, and Applications*, edited by D.V. Morgan (Wiley, New York, 1973), p. 100.
[15] J.U. Andersen, B. Bech Nielsen, A. Uguzzoni, E. Fuschini, E.F. Kennedy, and V.A. Ryabov, Nucl. Instrum. Methods Phys. Res. B **90**, 166 (1994).
[16] E. Bonderup, H. Esbensen, J.U. Andersen, and H.E. Schiott, Radiat. Eff. **12**, 261 (1972).
[17] H.E. Schiott, E. Bonderup, J.U. Andersen, and H. Esbensen, in *Atomic Collisions in Solids*, edited by S. Datz, B.R. Appleton, and C.D. Moak (Plenum Press, New York, 1975), Vol. 2, p. 843.
[18] J.P. Rozet, C. Stephan, and D. Vernhet, Nucl. Instrum. Methods Phys. Res. B **107**, 67 (1996).
[19] H.A. Bethe and E.E. Salpeter, *Quantum Mechanics of One and Two-Electron Atoms* (Academic Press, New York, 1957).
[20] Dz. Belkic, R. Gayet, and A. Salin, Comput. Phys. Commun. **32**, 385 (1984).
[21] R. Gayet (private communication).
[22] J.P. Rozet (private communication).
[23] J. Eichler, Phys. Rev. A **31**, 3505 (1985).

[24] W.E. Meyerhof, R. Anholt, J. Eichler, H. Gould, Ch. Munger, J. Alonso, P. Thieberger, and H.E. Wegner, Phys. Rev. A **32**, 3291 (1985).
[25] A. Salin (private communication).
[26] S. Andriamonje, M. Chevallier, C. Cohen, N. Cue, D. Dauvergne, J. Dural, F. Fujimoto, R. Kirsch, A. L'Hoir, J.C. Poizat, Y. Quéré, J. Remillieux, C. Röhl, H. Rothard, J.P. Rozet, D. Schmaus, M. Toulemonde, and D. Vernhet, Nucl. Instrum. Methods Phys. Res. B **107**, 3291 (1996).
[27] K. Omidvar, At. Data Nucl. Data Tables **28**, 1 (1983).
[28] M.O. Krause, J. Phys. Chem. Ref. Data **8**, 307 (1979).
[29] J. Lindhard and A.H. Sørensen, Phys. Rev. A **53**, 2443 (1996).
[30] C. Scheidenberger, H. Geissel, H.H. Mikkelsen, F. Nickel, S. Czajkowski, H. Folger, H. Irnich, G. Münzenberg, W. Schwab, T. Stöhlker, T. Suzuki, and B. Voss, Phys. Rev. Lett. **77**, 3987 (1996).
[31] J.R. Chelikowsky and M.L. Cohen, Phys. Rev. B **14**, 556 (1976).
[32] C. Scheringer, Acta Crystallogr., Sect. A: Found. Crystallogr. **36**, 205 (1980).
[33] S.M. Younger, Phys. Rev. A **24**, 1272 (1981).
[34] Y.-K. Kim and M.E. Rudd, Phys. Rev. A **50**, 3954 (1994).
[35] P. Indelicato (private communication).
[36] C.J. Fontes, D.H. Sampson, and H.L. Zhang, Phys. Rev. A **51**, R12 (1995).
[37] S.M. Younger, Phys. Rev. A **22**, 111 (1980); **22**, 1425 (1980).
[38] R.E. Marrs, S.R. Elliot, and D.A. Knapp, Phys. Rev. Lett. **26**, 4082 (1994).
[39] S. Datz, H.F. Krause, C.R. Vane, H. Knudsen, P. Grafström, and R.H. Schuch, Phys. Rev. Lett. **77**, 2925 (1996).
[40] J.L. Dehmer, M. Inokuti, and R.P. Saxon, Phys. Rev. A **12**, 102 (1975).
[41] J.F. Ziegler, *Handbook of Stopping Cross-Sections for Energetic Ions in All Elements* (Pergamon Press, New York, 1980).
[42] C. Scheidenberger, H. Geissel, H.H. Mikkelsen, F. Nickel, T. Brohm, H. Folger, H. Irnich, A. Magel, M.F. Mohar, G. Münzenberg, M. Pfützner, E. Roeckl, I. Schall, D. Schardt, K.-H. Schmidt, W. Schwab, M. Steiner, T. Stöhlker, K. Sümmerer, D.J. Viera, B. Voss, and M. Weber, Phys. Rev. Lett. **73**, 50 (1994).
[43] J.H. Scofield, Phys. Rev. A **18**, 963 (1978).